Fuel 182 (2016) 411–418

Contents lists available at ScienceDirect

Fuel

journal homepage: www.elsevier.com/locate/fuel

Full Length Article

Impact of iron porphyrin complexes when hydroprocessing algal HTL biocrude

Jacqueline M. Jarvis [a], Nilusha M. Sudasinghe [a], Karl O. Albrecht [b], Andrew J. Schmidt [b], Richard T. Hallen [b], Daniel B. Anderson [b], Justin M. Billing [b], Tanner M. Schaub [a,*]

[a] Chemical Analysis and Instrumentation Laboratory, College of Agricultural, Consumer and Environmental Sciences, New Mexico State University, 945 College Avenue, Las Cruces, NM 88003, USA
[b] Chemical and Biological Processes Development Group, Pacific Northwest National Laboratory, P.O. Box 999, Richland, WA 99352, USA

ARTICLE INFO

Article history:
Received 17 March 2016
Received in revised form 16 May 2016
Accepted 21 May 2016
Available online 6 June 2016

Keywords:
ICR
FT-ICR MS
HTL biocrude
Porphyrins
ICP
Algae
Iron porphyrins
Biofuel
Thermochemical processing

ABSTRACT

We apply Fourier transform ion cyclotron resonance mass spectrometry (FT-ICR MS) for direct characterization of iron-porphyrins in hydrothermal liquefaction (HTL) biocrude oils derived from two algae: *Tetraselmis* sp. and cyanobacteria. The iron porphyrin compounds are shown to cause catalyst bed plugging during hydroprocessing due to iron deposition. Inductively-coupled plasma optical emission spectrometry (ICP-OES) was utilized for iron quantitation in the plugged catalyst beds formed through hydroprocessing of the two HTL biocrudes and identifies an enrichment of iron in the upper five centimeters of the catalyst bed for *Tetraselmis* sp. (Fe = 100,728 ppm) and cyanobacteria (Fe = 115,450 ppm). Direct infusion FT-ICR MS analysis of the two HTL biocrudes with optimized instrument conditions facilitates rapid screening and identification of iron porphyrins without prior chromatographic separation. With FT-ICR MS we identify 138 unique iron porphyrin compounds in the two HTL biocrudes that have similar carbon number and double bond equivalent distributions to the metal porphyrins (e.g. Ni and V) reported for petroleum. No iron porphyrins are observed in the cyanobacteria HTL biocrude after hydroprocessing, which indicates that iron porphyrin structures in the HTL biocrude are degraded during hydrotreatment. Hydrodemetallization reactions that occur through hydroprocessing of HTL biocrudes could be responsible for the decomposition of iron porphyrin structures leading to metal deposition in the catalyst bed that result in catalyst deactivation and bed plugging, and must be addressed for effective upgrading of algal HTL biocrudes.

1. Introduction

Hydrothermal liquefaction (HTL) technology is a current forerunner for biomass-to-oil conversion for high-moisture feedstock. Algal HTL biocrude is substantially more complex than directly-harvested plant oils such as vegetable or palm oil and has elevated heteroatom content (i.e., N, O, P, S) that is addressed by hydroprocessing. Detailed characterization of all algal HTL products and process intermediates has been identified as a critical research need for technology advancement [1].

Unlike other thermochemical processes (e.g., pyrolysis, gasification), the HTL approach eliminates the energy requirement for water removal/drying of wet feedstock [2]. Through the HTL process biomass slurry at ~5–20% solids [3] is subjected to elevated temperature (280–370 °C) and pressure (10–25 MPa) to produce liquid hydrocarbon oil as a principal product with biochar solids, aqueous- and gas-phase by-products [4]. Algal hydrothermal liquefaction oil has an energy density comparable to that of petroleum crude (42 MJ/kg) with reported heating values of 40–50 MJ/kg (*Botryococcus brauni*) [5].

Catalytic hydrotreatment is the preferred method for removal of polar heteroatomic species from HTL biocrude. The process involves treatment of HTL biocrude with hydrogen (35–170 bar H_2) in the presence of heterogeneous catalysts (e.g. sulfided Co–Mo, Ni–Mo) at high temperature (300–450 °C) and liquid hourly space-velocity of 0.2–10 h^{-1} [6]. Catalytic hydrotreatment, though expensive, is also used by the petroleum industry for the removal of sulfur, nitrogen, oxygen, and metals from heavy petroleum fractions, and to saturate olefins and aromatic compounds. Catalytic hydrotreatment appears likely for commercial-scale biofuel production where existing infrastructure can be utilized for bio-oil treatment [6].

* Corresponding author.
E-mail address: tschaub@nmsu.edu (T.M. Schaub).

http://dx.doi.org/10.1016/j.fuel.2016.05.107
0016-2361/

Fast pyrolysis bio-oils are thermally unstable and plug hydrotreatment reactors unless they are first stabilized [7,8]. In contrast, HTL oils are thermally stable and can be directly upgraded without prior low-temperature stabilization [8]. Recently at Pacific Northwest National Laboratory (PNNL), continuous hydrotreatment of HTL biocrudes from lignocellulosic feedstocks (e.g., wood and corn stover where iron content is less than 35 ppm) has been performed for hundreds of hours on-stream without catalyst bed plugging necessitating run termination [9,10]. However, catalyst beds used to hydrotreat algal-derived HTL biocrudes (Fe > 700 ppm) have been found to plug after only tens of hours of continuous processing. Analysis of the catalyst reactor has shown unexpectedly high concentration of iron near the head of the catalyst beds in all cases.

Metal-containing species (e.g., porphyrins) in petroleum cause bed plugging, increase coke formation, deactivate catalysts during upgrading and stabilize water-in-oil emulsions [11–13]. Porphyrins have high thermal stability which makes them difficult to eliminate [13] and metals within porphyrin complexes rapidly degrade catalysts. Nickel and vanadium are the two most abundant metals found in porphyrin structures in petroleum crude oil and concentration of 20–100 ppm and 50–250 ppm, are observed [13–15]. Iron is also present at high concentration (150–1000 ppm) within petroleum-based oils. However, high iron content largely originates from pipeline rust and is not of geochemical significance [13].

Recently, FT-ICR MS has been used to identify problematic compounds for petroleum refining operations [16–19]. The isolation of organometallic complexes from heavy crude oil has been reported [20–24] along with subsequent characterization by mass spectrometry [25–28]. FT-ICR MS coupled with atmospheric pressure photoionization (APPI) or electrospray ionization (ESI) has been used to characterize nickel and vanadyl porphyrins from heavy petroleum crude oil and natural seeps [12,15,29–34]. Here, we apply electrospray ionization Fourier transform ion cyclotron resonance mass spectrometry (ESI FT-ICR MS) to identify organometallic complexes, specifically iron-containing porphyrins, for the first time within algal HTL biocrudes. These compounds are responsible for bed plugging observed during hydrotreatment of the algae HTL biocrude.

2. Materials and methods

2.1. HTL biocrude production

HTL biocrudes were produced in one of two bench-scale continuous flow reactor systems (see Fig. A1). The *Tetraselmis* sp. composite biocrude was derived from a series of five HTL tests performed in a hybrid reactor system that combines plug flow reactor (PFR) components with a small continuous stirred tank reactor (CSTR) [33]. The cyanobacteria feedstock was processed in a single test in a recently commissioned reactor system that was configured to bypass the CSTR and rely solely on a plug flow tubular reactor. For both systems, the feedstock slurry (17.0–27.3 wt.% DAF *Tetraselmis* sp., 14.7 wt.% DAF cyanobacteria) is brought to operating pressure (3000 psig target, actual pressure 2910–3070, average 2970 psig *Tetraselmis*, 2930 psig cyanobacteria) and continuously fed to the reactor system using dual Teledyne Isco syringe pumps. In the hybrid configuration, the slurry is heated in a tube-in-tube, oil jacketed heat exchanger, then brought to HTL reactor temperature (350 °C target, actual temperatures 339–350 °C, average 346 °C Tetraselmis, 344 °C cyanobacteria) in the CSTR. Rapid mixing in the CSTR facilitates heat transfer and accommodates product slurry swelling. The liquefied slurry then proceeds to a tubular reactor that provides the requisite residence time (liquid hourly space velocity (LHSV) was 2.2 L/L/h for *Tetraselmis* sp.). In the PFR-only system, the CSTR is bypassed and the first heat exchanger is used to increase the temperature to 325 °C before entering the main tubular reactor (LHSV was 2.5 L/L/h for cyanobacteria). Downstream of the reactors, solids are removed from the product stream in a settling and filtration vessel where precipitated minerals settle to the bottom while liquids pass overhead through a stainless steel filter. After solids removal, the product is cooled to 40–70 °C and collected in one of two oil jacketed separators/collection vessels. At timed intervals, one vessel is isolated from the system and product collection is directed to the other vessel. The isolated vessel is depressurized, the product is retrieved, and the gravity separable HTL biocrude is separated from the aqueous phase. The yield of gravity separable biocrude (no solvent extraction) as a percentage of the mass of DAF feed solids ranged from 34 to 45 wt.% for the *Tetraselmis* sp. tests and was 27 wt.% for the cyanobacteria test.

2.2. HTL biocrude hydroprocessing

HTL biocrude samples were hydroprocessed in a continuous mini-hydrotreater system at PNNL, as previously described by Elliott et al. [35]. Two HTL biocrudes (*Tetraselmis* sp. and cyanobacteria) were hydroprocessed in separate runs. The catalyst was identical for both tests, but the bed was configured differently in each case. The $CoMo/Al_2O_3$ catalyst (Alfa Aesar, Ward Hill, MA, USA. Product No. 45579) was supplied as extrudates in the oxide form and reported by the supplier to consist of 3.4–4.5% cobalt oxide and 11.5–14.5% molybdenum oxide on alumina. For the *Tetraselmis* sp. test, 20 mL/14.4 g of catalyst was ground and sieved to −30/+60 mesh and loaded into the reactor. On top of the catalyst bed, ~4 mL/2.1 g of catalyst was loaded as unground extrudate. For the cyanobacteria test, 12 mL/7.7 g of catalyst was ground to −30/+60 mesh on top of which another 12 mL/8.7 g of unground extrudate was added.

The catalyst was sulfided with 35 wt.% di-tertbutyl disulfide (DTBDS, Sigma Aldrich, St. Louis, MO, USA) in decane prior to the introduction of HTL biocrude for both tests. Next, the reactor was pressurized to 1500 psig with H_2 and the H_2 flow was allowed to stabilize prior to heating the reactor to 150 °C. The DTBDS/decane solution was introduced with a nominal flow rate of 0.16 mL solution/mL catalyst/h (volumetric flow rate determined at 21 °C). The volume of the extrudate and sized material was included in the catalyst volume calculation. Hydrogen gas was added at nominally 2000 SCCM/mL sulfiding solution. The temperature was then ramped at 1.4 °C/min to 400 °C and held for 4 h. The HTL biocrude was introduced to the reactor immediately after sulfiding.

Reactor conditions for the *Tetraselmis* sp. HTL biocrude hydrotreatment were nominally 400 °C and 1500 psig. The temperature profile of the bed was measured periodically at 2.5 cm intervals during the run via an internal thermowell. The volumetric feed rate of the HTL biocrude was 0.1 mL/min (measured at 40 °C). The mass flow rate of the HTL biocrude was 0.093 g/min (dry basis). Hydrogen gas was co-fed to the system at 125 SCCM. The *Tetraselmis* sp. HTL biocrude was processed for 102 h, after which a buildup of system pressure led to system shutdown. The system was then cooled, depressurized and the catalyst bed recovered. The observed plug was characterized as a hardened section of the catalyst bed that was solidified to the point that drilling was required to remove it. Extrudate above and sized catalyst below the plug were free flowing upon catalyst bed recovery.

The cyanobacteria hydroprocessing test utilized separate heat zones for the extrudate and sized portions of the catalyst bed. The nominal temperature for the extrudate bed portion was 370 °C. The temperature in the portion of the catalyst bed consisting of the sized catalyst particles was 400 °C. The temperature

profile of the bed was measured periodically via the internal thermowell. The nominal pressure was 1500 psig. For the cyanobacteria test, HTL biocrude was fed at a volumetric flow rate of 0.044 mL/min, or 0.041 g/min on a dry basis. H_2 was co-fed at 58 SCCM. The system was run until all available HTL biocrude was processed, which was 220 h on-stream. Upon completion of the run, the catalyst was cooled to 120 °C and acetone was passed through the reactor to remove residual organics. The bed was then recovered for analysis.

2.3. Ultimate and ICP-OES analysis

The HTL biocrude samples and hydrotreated organic products were analyzed for CHN (ASM D5373/D5291), O (modified ASTM D5373), S (ASTM D4239/D1552), moisture (Karl Fisher analysis, ASTM D6869) and total acid number (mg KOH/g; ASTM D3339) (Table A1). The sulfur concentration in the organic hydrotreated products (ppm level) was determined at PNNL following ASTM D5453. Simulated distillation of the organic products was also conducted following ASTM D2887. Trace element analysis was conducted via ICP-OES as described previously [36].

2.4. Mass spectrometry

The HTL biocrudes were dissolved in 50:50 chloroform:methanol (HPLC grade, Sigma Aldrich, St. Louis, MO) to create 1 mg/mL stock solutions. Final samples for direct infusion were diluted in methanol to 250 μg/mL with 1% formic acid for positive-ion electrospray analysis. Direct infusion mass spectrometry of *Tetraselmis* sp. and cyanobacteria HTL biocrudes was performed on a hybrid linear ion trap 7 T FT-ICR mass spectrometer (LTQ FT, Thermo, San Jose, CA). Positive-ion electrospray mass spectra were collected with either an Advion TriVersa NanoMate (Advion, Inc., Ithaca, NY) or micro-electrospray at a mass resolving power of ~390,000 at m/z 400. The tube lens voltage of 85 V was utilized to allow the optimal transfer of all ions of interest (m/z ~100–700) or adjusted to 185 V to view porphyrin ions preferentially.

Multiple 200 individual time-domain transients were co-added, Hanning-apodized, zero-filled, and fast Fourier transformed prior to frequency conversion to mass-to-charge ratio [37] to obtain the final mass spectrum. Transient length was ~3 s. All observed ions were singly charged, as evident from unit m/z spacing between species which differ by $^{12}C_c$ vs. $^{13}C_1{}^{12}C_{c-1}$.

Data were analyzed and peak lists generated with PetroOrg© software (Omics LLC). Internal mass calibration of mass spectra was based on homologous series whose elemental compositions differ by integer multiples of 14.01565 Da (i.e., CH_2) [38]. Compounds with the same heteroatom content (i.e., same number of n, o, and s in $C_cH_hN_nO_oS_s$) but differing in degree of alkylation may then be grouped [39]. Elemental formulae were assigned to peaks with signal to noise ratios greater than 10 and the broadband mass measurement error was 158 ppb and 287 ppb (rms) for the *Tetraselmis* sp. and cyanobacteria mass spectra, respectively.

3. Results and discussion

3.1. Hydroprocessing Issues

Figs. 1 and 2 show the reactor temperature profile and schematic for the hydroprocessing of *Tetraselmis* sp. and cyanobacteria HTL biocrudes, respectively. *Tetraselmis* sp. and cyanobacteria HTL biocrudes were both hydrotreated with Co–Mo catalyst beds, albeit under different conditions. The temperature profile for the *Tetraselmis* sp. run was measured after 90 h on stream. For the *Tetraselmis* sp. HTL biocrude, the catalyst bed formed a plug 0.6 cm from the top of the bed to about 5 cm within the bed depth after 102 h of operation and forced a shutdown of the system (~342–355 °C). The catalyst bed used for the hydroprocessing of the cyanobacteria HTL biocrude was operated continuously for 219.8 h (i.e., all HTL biocrude feed was exhausted) without a forced system shutdown by catalyst bed plugging. The temperature profile measured for the cyanobacteria test was conducted at about 208 h on stream.

3.2. ICP-OES analysis

The analysis of each catalyst bed upon shutdown of the hydroprocessing units showed deposits in the upper region of both catalysts beds. ICP-OES analysis was performed on three different regions of the catalyst bed (i.e., above the plug, at the plug and below the plug) used to hydrotreat the *Tetraselmis* sp. HTL biocrude (Fig. 1). Table 1 shows the metal quantitation by ICP-OES for the different regions of the *Tetraselmis* sp. catalyst bed. The ICP-OES results show a 47-fold and 118-fold higher Fe content (100,728 ppm) in the catalyst plug relative to the regions above (2162 ppm) and below (853 ppm) the plug. There are also high concentrations of Al, Co, Mo, and S in the catalyst bed; however, these metals make up the catalyst (sulfided Co–Mo on alumina support). Ergo, the ICP-OES metal quantitation of the catalyst bed will show high concentration of these metals.

Iron (1289 ppm) is the only metal present in a concentration > 1000 ppm in the *Tetraselmis* sp. HTL biocrude (Table 2). The next highest metal concentration in the biocrude is K (57 ppm), which is 22 times lower than the concentration of iron. The *Tetraselmis* sp. algae feed contains several metals (i.e., Ca, Fe, K, Mg, and Na) in high concentrations (>1000 ppm), but only Fe remains at a high concentration after the HTL process and is present in high enough concentrations to cause detrimental effects in the hydrotreatment unit. Subsequently, ICP-OES analysis of the upgraded *Tetraselmis* sp. HTL oil after hydroprocessing shows a significant reduction in Fe concentration (<20 ppm in upgraded oil) which corresponds to the increased deposition of Fe in the catalyst bed plug.

Although the catalyst bed from the hydrotreatment of cyanobacteria HTL biocrude did not plug, the catalyst bed was still divided into three regions (i.e., the top region of hard chunks mixed with extrudate = ~0.0–3.8 cm, the region of free flowing extrudates = ~3.9–10.2 cm, and the region of free flowing sized catalyst = ~10.3–20.4 cm) and material from each region was subjected to ICP-OES analysis (Fig. 2). For cyanobacteria, region 1 contained 115,450 ppm of Fe compared to 12,910 ppm and 6837 ppm of Fe in regions 2 and 3. Similar to *Tetraselmis* sp. biocrude, the cyanobacteria HTL biocrude also contained Fe (718 ppm) in the highest concentration (Table 2) which led to iron deposits in region 1 of the catalyst bed.

In both the *Tetraselmis* sp. and cyanobacteria hydrotreatment runs, higher Fe concentrations were found in the top ~5 cm of the catalyst beds. The plug in the *Tetraselmis* sp. reactor occurred from about 0.6 cm to about 5 cm in bed length. Hence, the deposition occurred from ~342 °C to ~355 °C (Fig. 1). In the case of the cyanobacteria, deposits and high Fe content were observed from 0.0 to 3.8 cm (region 1) in the catalyst bed. However, the temperature near the top of the catalyst bed was already at 366 °C (Fig. 2) for the cyanobacteria run. Therefore, it appears that iron deposition may be temperature dependent (e.g., the top 0.6 cm of the catalyst bed in the *Tetraselmis* sp. test was not part of the plug and showed a low level of deposited metals) and occurs between 342 °C and 360 °C based on the *Tetraselmis* sp. run data.

3.3. FT-ICR MS analysis of HTL biocrudes

Unprocessed *Tetraselmis* sp. and cyanobacteria HTL biocrudes were subjected to FT-ICR MS analysis to identify Fe-containing

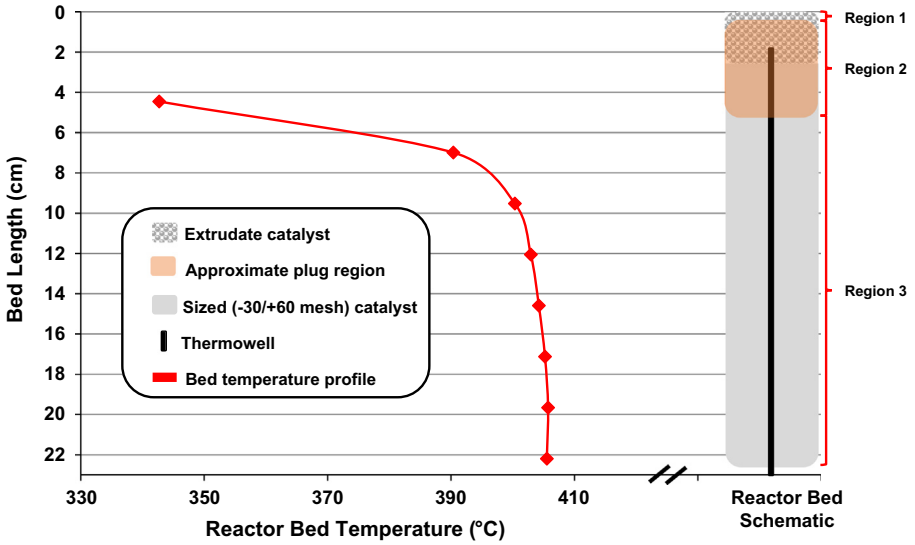

Fig. 1. *Tetraselmis* sp. hydrotreater temperature profile and reactor bed configuration with plug location.

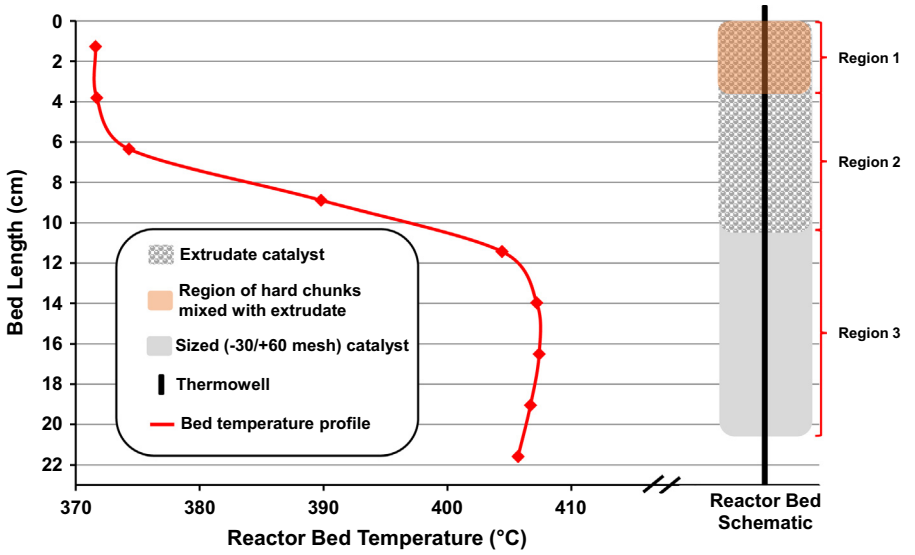

Fig. 2. Cyanobacteria hydrotreater temperature profile and reactor bed configuration.

organic species. Fig. 3 (top) shows the broadband, positive ion ESI FT-ICR mass spectra of *Tetraselmis* sp. and cyanobacteria HTL biocrudes where ultrahigh resolution and mass accuracy (inherent to FT-ICR MS) allows for the assignment of elemental compositions for several thousand compounds observed within each sample.

In addition to polar compound distribution that is similar to that previously described for algal HTL biocrudes (Fig. A2) [40,41], we observe numerous abundant peaks between m/z 450–600 that are identified as N_4Fe_1 species, with carbon and double bond content that are consistent with iron-porphyrins. An increase in the tube lens voltage within the MS ion source region (from the standard value of 85–185 V) increases ion kinetic energy and highlights ion signals for structurally robust molecules. Mass spectra collected with a tube lens voltage of 185 V (Fig. 3, bottom) show a distribution of peaks at m/z ~450–600 that are resistant to ion fragmentation at elevated tube lens voltage. The mass spectral signal-to-noise ratio (S/N) of porphyrins observed with a tube lens voltage of 185 V is higher than that observed with the tube lens voltage of 85 V by a factor of four, which illustrates that these species are not fragmented as a result of elevated tube lens voltage.

Additionally, chlorophyll was extracted from dried *Tetraselmis* sp. algae and mass spectra derived from that extract show similar distributions for both tube lens settings. Most importantly, the abundant peaks (i.e., chlorophyll a, chlorophyll b, pheophytin a, and hydroxypheophytin a), are observed at increased S/N for the mass spectra collected with a higher tube lens voltage which demonstrates that even porphyrins with large porphyrin substitutions (e.g., phytyl) remain intact with an elevated tube lens settings (Fig. A3). Thus, elevated tube lens voltage is a convenient means to rapidly screen for the presence of porphyrins in HTL biocrude samples.

Molecular formulae were assigned to each (+) ESI FT-ICR mass spectrum of algal HTL biocrude collected at tube lens voltage = 185 V with the constraints of C = 1–100, H = 4–200, N = 4–6, O = 0–10, Fe = 1–1. There were 84 and 67 iron-containing compounds assigned to the (+) ESI mass spectrum of unprocessed

Table 1
ICP-OES data from three zones within the recovered catalyst bed from the *Tetraselmis* sp. and cyanobacteria hydroprocessing test.

Element	*Tetraselmis* sp.			Cyanobacteria		
	Region 1 [above the plug] (ppm)	Region 2 [at the plug] (ppm)	Region 3 [below the plug] (ppm)	Region 1 (~0.0–3.8 cm) (ppm)	Region 2 (~3.9–10.2 cm) (ppm)	Region 3 (~10.3–20.4 cm) (ppm)
Al	262,050	180,450	356,950	134,750	257,800	246,300
Ca	451	379	506	2099	497	584
Co	26,430	18,242.5	35,005	12,525	25,720	25,235
Cr	<40	744	24	572	2288	160
Cu	<40	378	28	11,004	<40	<40
Fe	2162	100,728	853	115,450	12,910	6837
K	152	269	52	13,360	72	434
Mg	240	226	321	1677	215	388
Mn	<40	102	42	363	83	42
Mo	41,580	17,625	23,495	23,135	16,850	16,380
Na	254	591	90	74,400	233	627
Ni	101	3709	547	2587	1825	845
P	8788	5242	11,555	2910	7201	6505
S	57,465	120,775	58,265	108,300	55,400	50,125
Si	288	379	414	287	316	298
Zn	64	487	59	16,265	<40	94

Metal concentrations for *Tetraselmis* sp. hydroprocessing test are reported as averages of 2 (region 1), 4 (region 2) and 2 (region 3) replicate samples.

Table 2
ICP-OES data from the algae feeds (dry basis), biocrude, and upgraded oils. N/A = not analyzed.

Element	*Tetraselmis* sp.			Cyanobacteria		
	Algae feed [dry][a] (ppm)	Biocrude (ppm)	Upgraded oil[b] (ppm)	Algae feed [dry] (ppm)	Biocrude (ppm)	Upgraded oil (ppm)
Al	238–401	<35	<100	<30	<30	<15
Ca	15,938–22,765	<35	<30	8594	<30	<15
Co	N/A	<35	<10	<30	<30	<15
Cr	<35	<35	<10	<30	<30	<15
Cu	<35	<35	N/A	<30	19	<15
Fe	2138–2420	1289	<20	127	718	<15
K	15,035–16,283	57	<100	15,985	111	<30
Mg	6882–8659	<35	<100	7637	<30	<15
Mn	124–128	<35	N/A	<30	<30	<15
Mo	N/A	<35	<20	<30	<30	<15
Na	23,853–60,080	25	<100	47,005	257	<30
Ni	N/A	44	<10	<30	<30	<15
P	6400–8782	<35	<100	5403	<30	<15
S	9340–14,340	5426	N/A	11,255	7365	<20
Si	47–1561	36	<100	49	<30	<15
Zn	N/A	N/A	<15	N/A	N/A	<15

[a] Six HTL runs generated the biocrude composited used for this report. All of the feeds for the six runs had values between the ranges reported.
[b] Data from samples generated from a previous run at similar conditions with identical catalyst but without a guard bed section.

Tetraselmis sp. and cyanobacteria HTL biocrudes (Table A2). In total, 138 unique iron-containing porphyrin ions were observed, which consist of two ion types (i.e., iron cations (half-integer DBE) and protonated cations (integer DBE)), identified within HTL biocrudes derived from algae. The dominant species present in algae HTL biocrude belong to N_4Fe_1 species, although $N_{4-6}O_{0-3}Fe_1$ species were also identified.

Fig. 4 shows zoom insets of the (+) ESI FT-ICR mass spectrum obtained from the unprocessed *Tetraselmis* sp. HTL biocrude. The zoom inset of *m*/*z* 470–570 shows the dominant species in this region belong to DBE 17.5 and 18.5 N_4Fe_1 species (Fig. 4B). The identification of iron-porphyrin compatible elemental compositions was verified with sub-ppm mass accuracy throughout all the algae HTL biocrudes (Table A2). Fig. 4A shows a zoom inset (*m*/*z* 502–506) within the *Tetraselmis* sp. HTL biocrude which validates the assignment of iron-containing porphyrins. The dominant peak at *m*/*z* 504.19706 corresponds to the monoisotopic formula $C_{30}H_{32}N_4^{56}Fe^+$. The other two abundant peaks within this region belong to its ^{54}Fe and ^{13}C isotopologues (*m*/*z* 502.20176 and *m*/*z* 505.18482). The main ion type observed in this (+) ESI analysis of algae HTL biocrudes correspond to charged iron (III) complexes as observed by Kaczorowska and Cooper [42]. Less-abundant, protonated iron porphyrins correspond to iron (II) complexes have carbon number and DBE values that are analogous to those of the iron (III) species.

Fig. 5 shows the composite compositional space coverage (double bond equivalent distribution, DBE = number of rings + double bonds to carbon and carbon number distribution) of all the N_4Fe_1 species identified within *Tetraselmis* sp. and cyanobacteria HTL biocrudes. The N_4Fe_1 species range from C_{26}–C_{40} and DBE 17–22 with the most abundant species between C_{29}–C_{33} and DBE 17–18. While both the carbon number (C = 26–40) and DBE distribution (DBE = 17–22) of algal HTL biocrude iron porphyrins are quite similar to those of Ni- and V-porphyrins identified from petroleum and natural seeps (see Table 3) [12,15,33,34], mass spectrometry does not differentiate isomers, therefore it is possible that the algal HTL oil porphyrins are different isomers than those found in petroleum.

Fig. 6 shows the DBE distributions of N_4Fe_1 species ($S/N > 40$) isolated from *Tetraselmis* sp. and cyanobacteria HTL biocrudes. Etioporphyrin (ETIO) and deoxophylloerthroetioporphyrin (DPEP) structures (DBE = 17 and 18) have been identified as the most abundant porphyrin structures found in petroleum crude oil and natural seeps and are also the most abundant structures present in the algae HTL biocrudes we analyzed (Fig. 6). Structures that correspond to Rhodo-DPEP (DBE = 21) and di-DPEP (DBE = 19) por-

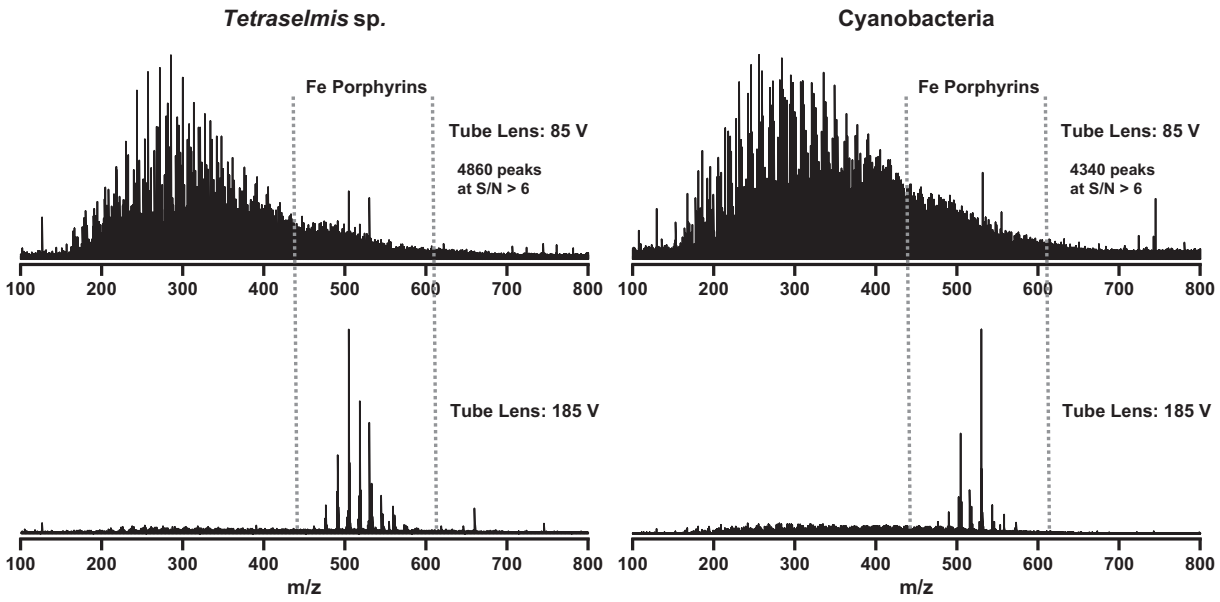

Fig. 3. Positive-ion ESI FT-ICR mass spectra of *Tetraselmis* sp. (left) and cyanobacteria (right) HTL biocrudes collected with a tube lens voltage of 85 V (top) and 185 V (bottom). Mass spectral signals for Fe porphyrins (m/z ~450–600) dominate each mass spectrum.

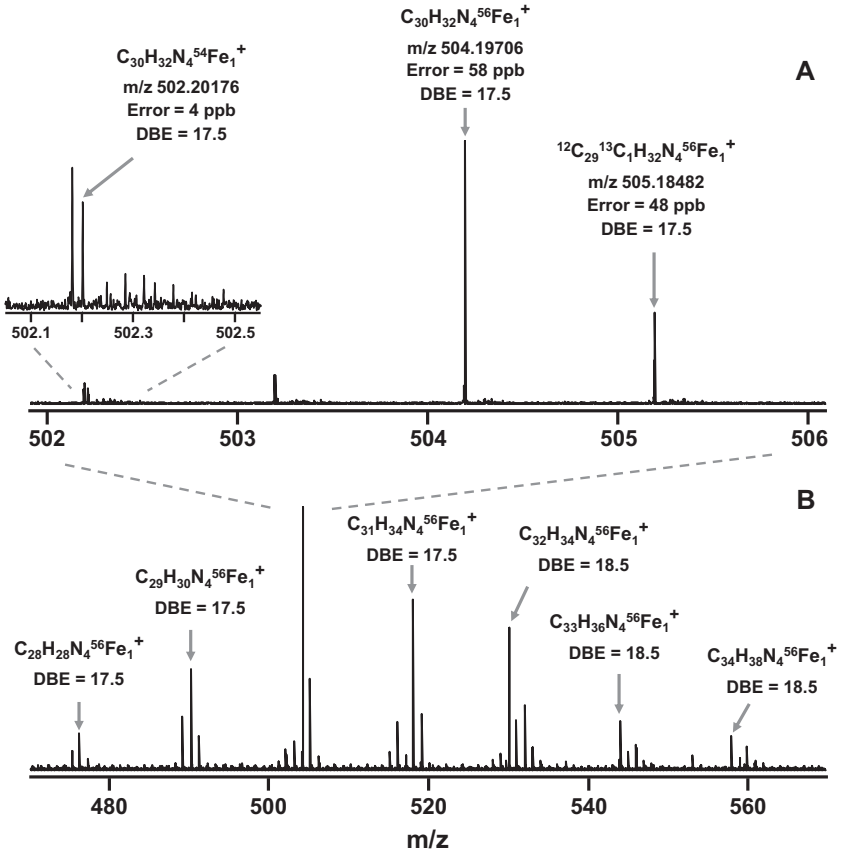

Fig. 4. Mass scale expanded segments of the broadband positive-ion ESI FT-ICR mass spectrum of the *Tetraselmis* sp. HTL biocrude collected with a tube lens voltage of 185 V. Mass segments at m/z 502–506 (A) and m/z 470–570 (B) highlight the mass spectral signals which correspond to Fe porphyrin species.

phyrins are also present in the algal HTL biocrudes. Interestingly, possible Rhodo-ETIO (DBE = 20) structures were not observed in any of the algal HTL biocrudes although N_4Fe_1, DBE = 20 species were observed in the catalyst bed. Notably, similar porphyrin structures were identified in other algae HTL biocrudes examined (e.g., *Chlorella* sp. and *Scenedesmus* sp.) and are not unique to the two HTL biocrudes discussed thus far (Fig. A4, Table A2). Ultimately, porphyrins and coordinated metals inherent to algae HTL biocrudes will need to be addressed for refinement of these fuel precursors.

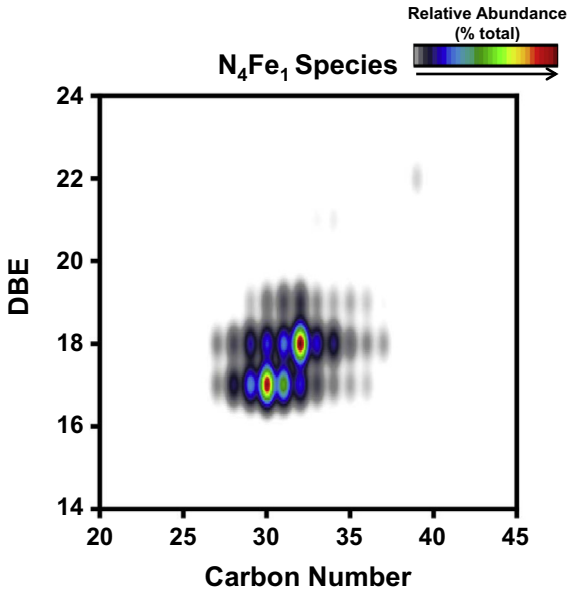

Fig. 5. Composite positive-ion ESI FT-ICR MS isoabundance-contoured plot of double bond equivalents (DBE = $c - h/2 + n/2 + 1$) versus number of carbons for all the members of the N_4Fe_1 class from *Tetraselmis* sp. and cyanobacteria HTL biocrudes.

Table 3
Reported porphyrin carbon number and DBE ranges.

Reference	Source petroleum	Porphyrin class	Carbon number range	DBE range
Liu et al. [12]	Heavy crude and bitumen resid	Ni and V	24–61	17–25
McKenna et al. [15]	Asphaltene and S. Am. Heavy Crude	V	26–45	16–23
Zhao et al. [33]	S. Am. Heavy Crude	V	25–59	17–22
McKenna et al. [34]	Natural oil seep	Ni and V	26–39	16–22
This study	Algal HTL oil	Fe	26–40	17–22

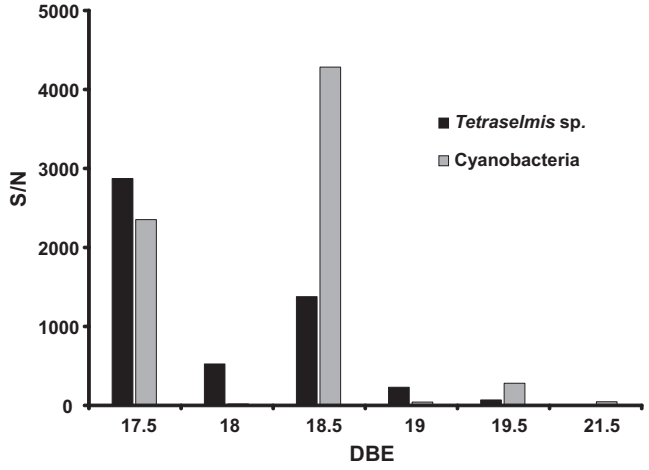

Fig. 6. Double bond equivalents (DBE) versus signal-to-noise ratios (*S*/*N*) for the members of the N_4Fe_1 class derived from the positive-ion ESI FT-ICR mass spectra of *Tetraselmis* sp. (black) and cyanobacteria (gray) HTL biocrudes. Half integer DBE values represent iron cations and integer DBE values represent protonated cations.

3.4. FT-ICR MS analysis of the Tetraselmis sp. catalyst bed

The toluene-soluble organics from the three different catalyst bed regions (i.e., above the plug, at the plug, and below the plug) used to hydroprocess the *Tetraselmis* sp. HTL biocrude were subjected to FT-ICR MS analysis. (Note: The cyanobacteria catalyst bed was washed with acetone after shutdown and not available for FT-ICR MS analysis.) For the region of the catalyst bed immediately upstream of the plug, the dominant mass spectral signals observed are those from iron-containing porphyrins (see Fig. A5). In addition to the dominant N_4Fe_1 species identified in the biocrude, $N_5O_1Fe_1$ and $N_8O_2Fe_2$ species were also present in the region of the catalyst bed above the plug. These species are the combination of the dominant N_4Fe_1 porphyrins with other abundant organics present in the biocrude (e.g., N_1O_1 species). We confirm that observation with MS^2 that shows precursor ions (for example, $N_5O_1Fe_1$, Fig. A6) that generate N_4Fe_1 product ions. The relative abundance of porphyrins is significantly less at the bed plug (~8%) and below the bed plug (~5%) relative to the region above the bed plug (~41%), which suggests that porphyrins are degraded and bound at the at the plug which results in iron deposition in the catalyst bed below 0.5 cm. Other abundant organic species extracted from the *Tetraselmis* sp. catalyst bed at the plug include N_1O_1 and N_2O_2 species (and N_1 and N_2 species below the plug).

3.5. The fate of iron-porphyrins during hydroprocessing

Fig. 7 compares (+) ESI FT-ICR mass spectra of cyanobacteria HTL biocrude before and after hydroprocessing. The distribution of porphyrin structures that were dominant mass spectral features for the unprocessed HTL biocrude at *m*/*z* 475–575 (Fig. 7, top) are not present in the hydroprocessed HTL biocrude (Fig. 7, bottom). The dominant species present in the hydrotreated biocrude are N_1 species, which are also present in the unprocessed biocrude along with iron porphyrins. Therefore, the absence of porphyrins in the hydroprocessed biocrude is not a result of ion suppression and indicates that the iron-porphyrin structures are degraded under hydrodemetallization (HDM) reactions that occur during hydrotreatment. Several reactions are known for HDM of nickel and vanadium porphyrins over $CoMo/Al_2O_3$ catalysts, where the porphyrin structure is first hydrogenated followed by hydrogenolysis that results in ring-opening and demetallization [43–47]. A similar mechanism may be responsible for the degradation of

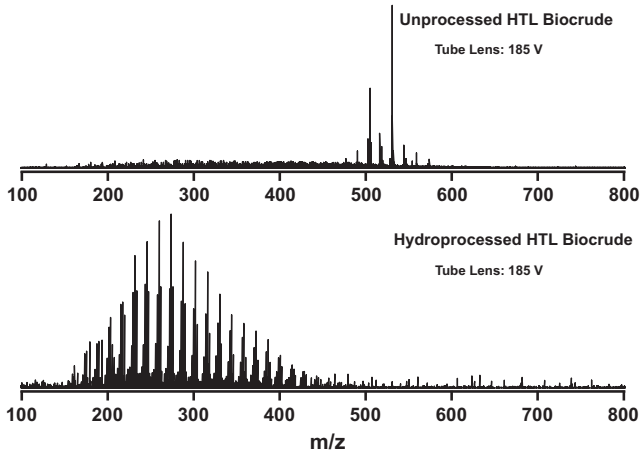

Fig. 7. Positive-ion ESI FT-ICR mass spectra of the unprocessed (top) and hydroprocessed (bottom) cyanobacteria HTL biocrude collected with a tube lens voltage of 185 V. Mass spectral signals for Fe porphyrins (*m*/*z* ~475–575) are absent in the hydroprocessed HTL biocrude.

iron-porphyrins in HTL biocrudes through hydroprocessing. Additionally, HDM reactions have been shown in the petroleum industry setting to be responsible for metal deposition in the catalyst bed causing catalyst deactivation and bed plugging [48], similar to that observed here for algal HTL biocrude hydroprocessing. Our results suggest that HDM reactions occur during hydrotreatment of algal HTL biocrude; however, more testing is needed to determine the exact mechanism of porphyrin degradation from our hydroprocessing conditions.

4. Conclusion

The deposition of iron in catalyst beds upon the hydroprocessing of algal HTL biocrudes was shown to be derived from organometallic compounds intrinsic to algal HTL biocrudes. In practice, the presence of catalyst and/or reducing atmosphere may facilitate decomposition of the porphyrin structure through HDM reactions and catalyst-facilitated decomposition is suggested by the presence of the metal deposits observed 3.8 cm deep into the catalyst bed during the cyanobacteria run. Metal deposition may deactivate the catalyst via a pore plugging mechanism [48] and as the catalyst deactivates, porphyrin-rich HTL biocrude may traverse further into the catalyst bed prior to decomposition and ultimate metal deposition. More testing is required to understand the thermal versus environmentally-facilitated (i.e., catalyst presence and reducing atmosphere) porphyrin decomposition mechanism.

Additionally, the deposition of iron in the top 5 cm of either catalyst bed indicates that iron-porphyrins deposit at a temperature range from ~340 °C and as high as ~360 °C. The cyanobacteria oil likely did not plug whereas the *Tetraselmis* sp. oil did was likely due to two factors. First, the total flow rate of oil was lower for the cyanobacteria test resulting in less total iron for deposition in the reactor. Second, the extended bed of catalyst extrudates in the reactor was designed to be "guard bed" where iron could deposit but oil could still flow around the less-tightly packed bed. Further testing is required to understand the exact mechanism for porphyrin degradation and iron deposition during algae HTL hydroprocessing.

Finally, the iron porphyrins identified in algal HTL biocrudes are similar in carbon number and DBE to the organometallic porphyrins identified from petroleum and natural seeps. These compounds will be present for all HTL biocrudes derived from photosynthetic organisms and production designs that reduce their presence should be considered (e.g., algal cultivation with minimized metal content in nutrient amendments).

Acknowledgments

This work was supported by the U.S. Department of Energy's Office of Energy Efficiency and Renewable Energy (Bioenergy Technologies Office), the United States National Science Foundation (IIA-1301346) and the Center for Animal Health and Food Safety at New Mexico State University.

Appendix A. Supplementary material

Supplementary data associated with this article can be found, in the online version, at http://dx.doi.org/10.1016/j.fuel.2016.05.107.

References

[1] Biddy M, Davis R, Jones S, Zhu Y. Whole algae hydrothermal liquefaction technology pathway: technical report; NREL/TP-5100-58051; PNNL-22314. Washington, D.C.: U.S. Dept. of Energy; 2013.
[2] Duan P, Savage PE. Ind Eng Chem Res 2011;50(1):52–61.
[3] Garcia Alba L, Torri C, Samorì C, van der Spek J, Fabbri D, Kersten SRA, et al. Energy Fuels 2011;26(1):642–57.
[4] Barreiro DL, Prins W, Ronsse F, Brilman W. Biomass Bioenergy 2013;53:113–27.
[5] Dote Y, Sawayama S, Inoue S, Minowa T, Yokoyama S. Fuel 1994;73(12):1855–7.
[6] Huber GW, Corma A. Angew Chem Int Ed 2007;46(38):7184–201.
[7] Baker EG, Elliott DC. In: Research in thermochemical biomass conversion. Springer; 1988. p. 883–95.
[8] Elliott DC. Energy Fuels 2007;21(3):1792–815.
[9] Elliott DC, Biller P, Ross AB, Schmidt AJ, Jones SB. Bioresour Technol 2015;178:147–56.
[10] Elliott D, Hallen R, Schmidt A. In: DOE bioenergy technologies office (BETO) 2015 project peer review, Alexandria, VA; 2015.
[11] Lee RF. Spill Sci Technol Bull 1999;5(2):117–26.
[12] Liu H, Mu J, Wang Z, Ji S, Shi Q, Guo A, et al. Energy Fuels 2015;29(8):4803–13.
[13] Speight JG. Handbook of petroleum analysis. In: Winefordner JD, editor. Chemical analysis. New York, NY: Wiley-Interscience; 2001.
[14] Ali MF, Abbas S. Fuel Process Technol 2006;87(7):573–84.
[15] McKenna AM, Purcell JM, Rodgers RP, Marshall AG. Energy Fuels 2009;23(4):2122–8.
[16] Marshall AG, Rodgers RP. Acc Chem Res 2004;37(1):53–9.
[17] Lobodin VV, Nyadong L, Ruddy BM, Curtis M, Jones PR, Rodgers RP, et al. Int J Mass Spectrom 2014.
[18] Purcell JM, Merdrignac I, Rodgers RP, Marshall AG, Gauthier T, Guibard I. Energy Fuels 2010;24(4):2257–65.
[19] Schaub TM, Jennings DW, Kim S, Rodgers RP, Marshall AG. Energy Fuels 2007;21(1):185–94.
[20] Marquez N, Ysambertt F, De La Cruz C. Anal Chim Acta 1999;395(3):343–9.
[21] Fish RH, Komlenic JJ, Wines BK. Anal Chem 1984;56(13):2452–60.
[22] Yin C-X, Stryker JM, Gray MR. Energy Fuels 2009;23(5):2600–5.
[23] Reynolds JG, Biggs WR. Acc Chem Res 1988;21(9):319–26.
[24] Biggs WR, Fetzer JC, Brown RJ, Reynolds JG. Liq Fuels Technol 1985;3(4):397–421.
[25] Johnson JV, Britton ED, Yost RA, Quirke JME, Cuesta LL. Anal Chem 1986;58(7):1325–9.
[26] Hajibrahim SK, Quirke JME, Eglinton G. Chem Geol 1981;32(1):173–88.
[27] Faramawy S, El-Sabagh SM, Moustafa YM, El-Naggar AY. Pet Sci Technol 2010;28(6):603–17.
[28] Wright BW, Smith RD. Org Geochem 1989;14(2):227–32.
[29] Qian K, Mennito AS, Edwards KE, Ferrughelli DT. Rapid Commun Mass Spectrom 2008;22(14):2153–60.
[30] Putman JC, Rowland SM, Corilo YE, McKenna AM. Anal Chem 2014;86(21):10708–15.
[31] Qian K, Edwards KE, Mennito AS, Walters CC, Kushnerick JD. Anal Chem 2010;82(1):413–9.
[32] Rodgers RP, Hendrickson CL, Emmett MR, Marshall AG, Greaney M, Qian K. Can J Chem 2001;79(5–6):546–51.
[33] Zhao X, Liu Y, Xu C, Yan Y, Zhang Y, Zhang Q, et al. Energy Fuels 2013;27:2874–82.
[34] McKenna AM, Williams JT, Putman JC, Aeppli C, Reddy CM, Valentine DL, et al. Energy Fuels 2014;28(4):2454–64.
[35] Elliott DC, Wang H, French R, Deutch S, Iisa K. Energy Fuels 2014;28(9):5909–17.
[36] Elliott DC, Hart TR, Schmidt AJ, Neuenschwander GG, Rotness LJ, Olarte MV, et al. Algal Res 2013;2(4):445–54.
[37] Ledford Jr EB, Rempel DL, Gross ML. Anal Chem 1984;56:2744–8.
[38] Kendrick E. Anal Chem 1963;35:2146–54.
[39] Hughey CA, Hendrickson CL, Rodgers RP, Marshall AG, Qian K. Anal Chem 2001;73(19):4676–81.
[40] Sudasinghe N, Dungan B, Lammers P, Albrecht K, Elliott D, Hallen R, et al. Fuel 2014;119:47–56.
[41] Faeth JL, Jarvis JM, McKenna AM, Savage PE. AIChE J 2015:1.
[42] Kaczorowska Ma, Cooper HJ. Chem Commun 2011;47(1):418–20.
[43] Hung C-W, Wei J. Ind Eng Chem Process Des Dev 1980;19(2):250–7.
[44] Hung C-W, Wei J. Ind Eng Chem Process Des Dev 1980;19(2):257–63.
[45] Agrawal R, Wei J. Ind Eng Chem Process Des Dev 1984;23(3):505–14.
[46] Ware RA, Wei J. J Catal 1985;93(1):100–21.
[47] Ware RA, Wei J. J Catal 1985;93(1):122–34.
[48] Galiasso R, Blanco R, Gonzalez C, Quinteros N. Fuel 1983;62(7):817–22.